Journal of Medicinal Chemistry Article

J. Med. Chem. **2010,** *53,* 7613–7624 **7613**
DOI: 10.1021/jm1009296

Nuclear Permeable Ruthenium(II) β-Carboline Complexes Induce Autophagy To Antagonize Mitochondrial-Mediated Apoptosis

Caiping Tan,[†] Sensen Lai,[†] Shouhai Wu,[†] Sheng Hu,[§] Lingjun Zhou,[†] Yu Chen,[†] Minxu Wang,[†] Yiping Zhu,[†] Wu Lian,[†] Wenlie Peng,[†] Liangnian Ji,[‡] and Anlong Xu*,[†]

[†]*State Key Laboratory of Biocontrol, Department of Biochemistry, College of Life Sciences, Sun Yat-sen University, Guangzhou, Guangdong 510006, P. R. China,* [‡]*MOE Laboratory of Bioinorganic and Synthetic Chemistry, School of Chemistry and Chemical Engineering, Sun Yat-sen University, Guangzhou 510275, P. R. China, and* [§]*Faculty of Chemical Engineering and Light Industry, Guangdong University of Technology, Guangzhou 510006, P. R. China*

Received July 22, 2010

The role of autophagy in cancer development and response to cancer therapy has been a subject of debate. Here we demonstrate that a series of ruthenium(II) complexes containing a β-carboline alkaloid as ligand can simultaneously induce autophagy and apoptosis in tumor cells. These Ru(II) complexes are nuclear permeable and highly active against a panel of human cancer cell lines, with complex **3** displaying activities greater than those of cisplatin. The antiproliferative potentialities of **1**−**3** are in accordance with their relative lipophilicities, cell membrane penetration abilities, and in vitro DNA binding affinities. Complexes **1**−**3** trigger release of reactive oxygen species (ROS) and attenuation of ROS by scavengers reduced the sub-G1 population, suggesting ROS-dependent apoptosis. Inhibition of ROS generation also reduces autophagy, indicating that ROS triggers autophagy. Further studies show that suppression of autophagy using pharmacological inhibitors (3-methyladenine and chloroquine) enhances apoptotic cell death.

Introduction

Autophagy, or type II programmed cell death, has been proposed as a third mode of cell death besides apoptosis and necrosis.[1,2] Autophagy is a double-edged sword in oncology, as it is involved in both cell survival and cell death. It is long known to provide a survival advantage to rapidly growing cells under conditions of hypoxic or metabolic stresses, which thus contributes to normal and cancer cell survival. It also has a role in the suppression of tumor growth, and autophagy defects are associated with increased tumorigenesis.[3,4] The role of autophagy in cancer therapy is also a topic of intense debate, and autophagy can serve as a cell survival pathway by suppressing apoptosis; thus, treating cancer cells by autophagy inhibition is possible.[5] It can also lead to death itself; thus, drugs can activate autophagy to kill cancer cells resistant to apoptosis.[6] As autophagy is such a fundamental process, establishing how the functional status of autophagy influences the response to cancer treatment is important.[4,7]

The development of metal complexes with bioactive molecules as ligands offers possibilities for the discovery of novel anticancer drugs with enhanced and targeted activity.[8] Substitution of the β-phenyl ring of tamoxifens by ferrocenyl group affords ferrocifens, which exhibit a strong antiproliferative effect in hormone-independent breast cancer cells, where tamoxifen and ferrocene are inactive.[9] The combination of Ru(II) arene complexes with staurosporine, a potent inhibitor for various kinases, results in the discovery of nanomolar and even picomolar protein kinase inhibitors,[10] and notably, the GSK-3β inhibitor DW1/2 is highly cytotoxic in vitro and can induce p53-activated apoptosis via the mitochondrial pathway in otherwise highly chemoresistant melanoma cells.[11]

Previously, a number of ruthenium compounds have been shown to display promising anticancer activity. Two Ru(III) complexes have successfully entered clinical trials, namely, NAMI-A[12] ([ImH][*trans*-$RuCl_4$(DMSO)(Im)], where Im = imidazole and DMSO = dimethylsulfoxide)[a] and KP1019[13] ([IndH][*trans*-$RuCl_4(Ind)_2$], where Ind = indazole). Ru(II) complexes carrying labile ligands such as "half-sandwich" arene complexes exhibit both in vitro and in vivo activities.[14,15] Some of the α-[Ru(II)$(azpy)_2Cl_2$] (azpy = 2-(phenylazo)-pyridine) type complexes show a cytotoxic potency similar to or even better than that of cisplatin.[16] It has also been reported that coordinatively saturated Ru(II) polypyridyl complex [Ru$(bpy)_2$(dppn)]Cl_2 (dppn = 4,5,9-16-tetraazadibenzo[*a*,*c*]naphthacene) exhibits cytotoxic activity against two cancer cell lines at low micromolar IC_{50} values.[17]

The β-carboline alkaloids are a class of synthetic and naturally occurring compounds that possess a large spectrum

*To whom correspondence should be addressed. Phone/Fax: 86-20-3933-2990. E-mail: lssxal@mail.sysu.edu.cn.

[a] Abbreviations: 1-Py-βC, 1-(2-pyridyl)-β-carboline; 3-MA, 3-methyladenine; AO, acridine orange; AVOs, acidic vesicular organelles; azpy, 2-(phenylazo)pyridine; bpy, 2,2′-bipyridine; CCCP, carbonyl cyanide *m*-chlorophenylhydrazone; CDKs, cyclin-dependent kinases; CQ, chloroquine; DIP, 4,7-diphenyl-1,10-phenanthroline; CT-DNA, calf thymus DNA; DMSO, dimethylsulfoxide; dppn, 4,5,9-16-tetraazadibenzo[*a*,*c*]naphthacene; dppz, dipyrido[3,2-*a*:2′,3′-*c*]phenazine; GF-AAS, graphite furnace atomic absorption spectrometry; H_2DCF-DA, 2′,7′-dichlorofluorescein diacetate; Im, imidazole; Ind, indazole; JC-1, 5,5′,6,6′-tetrachloro-1,1′,3,3′-tetraethylbenzimidazolylcarbocyanine iodide; MLCT, metal-to-ligand charge transfer; MMP, mitochondrial membrane potential; MTT, 3-(4,5-dimethylthiazol-2-yl)-2,5-diphenyltetrazolium bromide; NAC, *N*-acetylcysteine; PBS, phosphate buffered saline; phen, 1,10-phenanthroline; ROS, reactive oxygen species; TEM, transmission electron microscopy; Tiron, 4,5-dihydroxy-1,3-benzenedisulfonic acid disodium salt.

Published on Web 10/19/2010

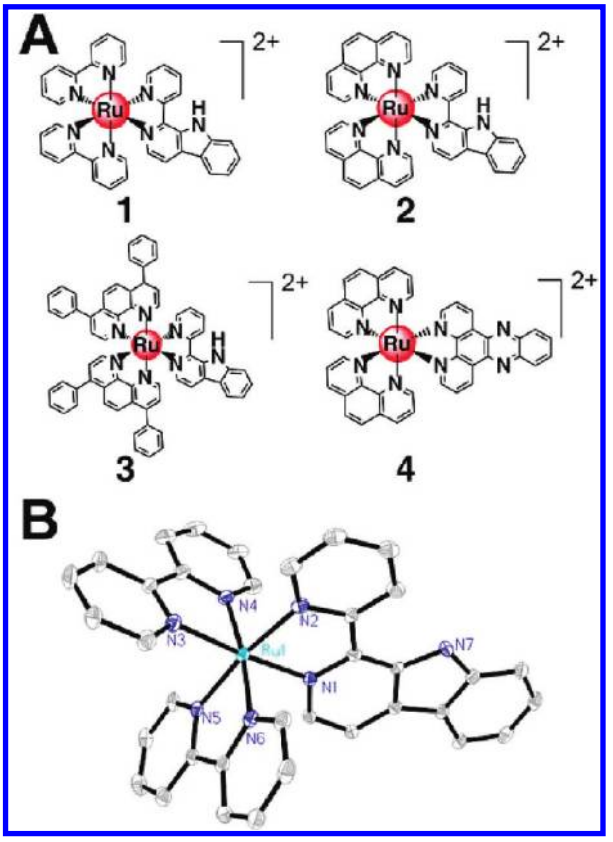

Figure 1. (A) Structures of the Ru(II) complexes. (B) ORTEP view of **1** (30% probability ellipsoids). Hydrogen atoms, solvated molecules, and anions are omitted for clarity.

of important pharmacological properties including sedative, anxiolytic, hypnotic, anticonvulsant, antitumor, antiviral, antiparasitic, and antimicrobial activities.[18] It has been reported that β-carboline alkaloids can exert antitumor activities through multiple mechanisms, such as intercalating into DNA[19] and inhibiting topoisomerases I and II,[20] CDKs (cyclin-dependent kinases),[21] and IκB kinases.[22] Various synthetic derivatives with different substituents in positions 1, 3, and 9 of the β-carboline skeleton have been synthesized in order to elucidate the structure−activity relationship of this class of compounds.[18] Al-Allaf and co-workers have reported the synthesis and the preliminary biological results of some Pd(II) and Pt(II) complexes based on monodentate β-carboline alkaloids.[23] The Pd(II) complex *trans*-[Pd(DMSO)(harmine)-Cl_2] shows a potency better than those of cisplatin, fluorouracil and carboplatin, while the mechanism of antitumor action by these complexes still remains largely speculative.[24]

The objective of the present study is to investigate the potential of ruthenium β-carboline complexes as anticancer drugs. Three luminescent Ru(II) complexes, $[Ru(N-N)_2(1\text{-Py-}\beta C)](PF_6)_2$ (N−N = 2,2′-bipyridine (bpy, **1**), 1,10-phenanthroline (phen, **2**), 4,7-diphenyl-1,10-phenanthroline (DIP, **3**); 1-Py-βC = 1-(2-pyridyl)-β-carboline) (Figure 1A), have been synthesized and characterized. $[Ru(phen)_2(dppz)](PF_6)_2$ (**4**, dppz = dipyrido[3,2-*a*:2′,3′-*c*]phenazine), which lacks a β-carboline moiety compared with **2**, is used as a reference in biological assays to investigate whether the biological activities of these complexes are associated with the β-carboline moiety. We show for the first time that Ru(II) complexes can induce autophagy and apoptosis simultaneously in HeLa (human cervical cancer) cells through a ROS (reactive oxygen species) mediated mechanism. Autophagy caused by **1**−**3** is detected by TEM (transmission electron microscopy) and analysis of the localization of green fluorescent protein-tagged autophagic marker microtubule-associated protein light chain 3 (GFP-LC3) in transfected HeLa cells. Inhibition of autophagy by pretreatment with 3-methyladenine (3-MA) or chloroquine (CQ) sensitizes the cells to apoptotic cell death, revealing that Ru(II)-induced autophagy plays a cytoprotective role. Additionally, confocal microscopy studies show that **3** can penetrate the nuclear envelope, making it possible that the primary target of these complexes is genomic DNA, so the binding of **1**−**3** with DNA has been studied by absorption and fluorescence spectroscopic studies to further elucidate whether the mechanism of **1**−**3** involves direct DNA damage.

Results

Synthesis and Characterization. The synthesis of the complexes $[Ru(N-N)_2(1\text{-Py-}\beta C)](PF_6)_2$ (**1**−**3**) was carried out as follows: (i) Synthesis of the ligand 1-Py-βC was achieved by reacting tryptamine and 2-pyridinecarboxaldehyde in dry anisole; (ii) $[Ru(N-N)_2(1\text{-Py-}\beta C)](PF_6)_2$ (**1**−**3**) were synthesized by refluxing 1 equiv of 1-Py-βC and *cis*-$[Ru(N-N)_2Cl_2]\cdot 2H_2O$ in 75% (v/v) aqueous ethanol for >3 h, followed by anion exchange with NH_4PF_6, purification by column chromatography, and recrystallization. The complexes were obtained as racemic mixtures containing both Δ- and Λ-isomers. The ligand and the complexes were characterized by ^{1}H NMR spectroscopy, ESI-MS (Supporting Information Figures S2−S9), and elemental analysis.

Complexes **1**−**3** show intense spin-allowed intraligand (^{1}IL) absorption bands in the UV region at approximately 250−340 nm and less intense spin-allowed metal-to-ligand charge transfer (^{1}MLCT) absorption bands at approximately 350−530 nm (Supporting Information Figure S10), which are typical absorption properties of Ru(II) polypyridine complexes. **1**−**3** display luminescence (550−700 nm) in Tris-HCl buffer at 298 K upon excitation at 488 nm. The emission maxima of all the complexes occur at approximately 604−609 nm (Figure 9B). The emission is attributed to a ^{3}MLCT ($d\pi(Ru) \rightarrow \pi^*$(diimine)) excited state.[25] The DIP complex **3** displays more intense emission than **1** and **2** do, and the reason is that the π* orbitals of DIP are lying in lower energy than bpy and phen, owing to the electron-withdrawing phenyl substitutions.[26]

The X-ray crystal structures of 1-Py-βC and complex **1** are depicted in Figure S1 (Supporting Information) and Figure 1B, respectively. The crystallographic data and selected bond lengths and angles are listed in Tables S1 and S2 (Supporting Information), respectively. The Ru(II) center of complex **1** adopts a distorted octahedral geometry, and the average Ru−N bond length is 2.059 Å, which is comparable to those found for $[Ru(bpy)_3]^{2+}$ (2.056 Å) and related compounds.[27] The average bite angle of bpy (87.10(13)°) falls within the same range as those of related tris(diimine)-ruthenium(II) complexes.[27,28]

Cellular Uptake. The cellular uptake properties of metal-based anticancer drugs are important factors that can influence their antiproliferative efficacies. For platinum complexes, increasing lipophilicities enhances the rate of cellular uptake and, consequently, the cytotoxic activities.[29] The cellular uptake characteristics of Ru(II) complexes can be estimated by their lipophilicities, which are commonly

referred to as the *n*-octan-1-ol/water partition coefficients (expressed as log $P_{o/w}$).[26,30] The log $P_{o/w}$ values of **1**−**3** were determined by reversed-phase HPLC (Supporting Information). The lipophilicities of the complexes are substantially increased by incorporating more hydrophobic ligand DIP, and the log $P_{o/w}$ value of the DIP complex **3** (3.39) is much larger than those of **1** (0.52) and **2** (1.43). The high lipophilicity of the DIP complex is anticipated to facilitate the tissue and cellular uptake.

Because of their stability in aqueous solution and luminescence (the luminescence intensity is increased upon binding with DNA, Figure 9B), the cellular uptake properties of Ru(II) polypyridyl complexes can be studied using flow cytometry and confocal microscopy conveniently.[26,30,31] First, flow cytometry was used to obtain semiquantitative data on the uptake of Ru(II) complexes into HeLa cells (Figure 2A). Cells not treated with Ru(II) exhibit neglectable background luminescence. Incubation with 20 μM complexes for 2 h causes changes in the luminescence profiles in the following order: **3** > **2** > **1**. The luminescence intensity of the cell population increases dramatically after cells are incubated for 2 h with 20 μM **3**. The time-dependent uptake profiles of **1**−**3** have also been measured (Supporting Information Figure S11). The complexes have accumulated in HeLa cells in 30 min. In addition, either lowering the incubation temperature or depleting the cellular ATP with CCCP (carbonyl cyanide *m*-chlorophenylhydrazone) shows little influence on uptake (Supporting Information Figure S12), which leads us to conclude that uptake might occur via an energy-independent process, i.e., passive diffusion, as proposed for $[Ru(DIP)_2(dppz)]Cl_2$.[31]

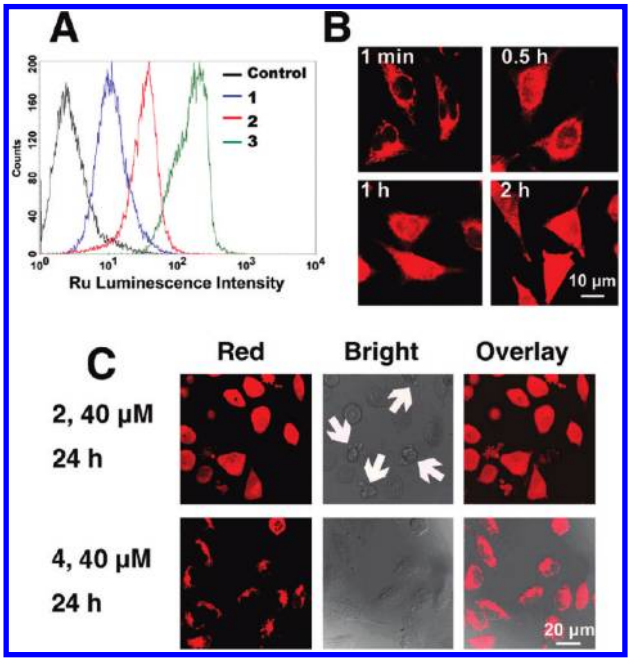

Figure 2. (A) Flow cytometric results of HeLa cells incubated with blank medium and complexes **1** (20 μM), **2** (20 μM), and **3** (20 μM) at 37 °C for 2 h. 10 000 events were collected in the FL2 channel (excitation, 488 nm; emission, 585 ± 21 nm). (B) Confocal images of HeLa cells treated with **3**. Cells were incubated with 5 μM complex **3** for different time intervals at 37 °C and observed by confocal microscopy (excitation, 488 nm; emission, 600−630 nm). (C) Comparison of the cellular localization of **2** and **4** taken by confocal microscopy (excitation, 488 nm; emission, 600−630 nm). Note the morphological changes (cell shrinkage and membrane blebbing) caused by treatment of **2** (indicated by arrows).

Flow cytometry cannot discriminate among membrane-associated, cytoplasmic, and nuclear localization, while the cellular localization characteristics of anticancer drugs are fundamental to their efficacy,[32,33] thus the cellular distribution Ru(II) has been studied by confocal microscopy. Interestingly, unlike $[Ru(DIP)_2(dppz)]Cl_2$, of which almost no nuclear staining can be observed,[26] complex **3** (5 μM) gradually penetrates into the interior of the nucleus and shows diffuse cytoplasmic and nuclear fluorescence after 2 h of incubation with HeLa cells (Figure 2B). The impact of the incorporation of 1-Py-βC on cellular distribution of Ru(II) complexes has been further investigated by using **4** as a reference, which lacks the β-carboline moiety. After incubation at 40 μM for 24 h, **2** produces a diffuse cytoplasmic and nuclear fluorescence in HeLa cells. In contrast, **4** accumulates in the cytoplasm and is predominantly excluded from the nucleus. Notably, cells treated with **2** show marked morphological changes (e.g., cell shrinkage and membrane blebbing).

The cellular ruthenium content of the samples was also determined by GF-AAS (graphite furnace atomic absorption spectrometry) quantitatively using the literature method.[17] The protein content was determined by the Bradford method, and results were reported as ng of ruthenium per mg of cellular protein. The uptake levels are relatively low for complexes **1** (148.1 ± 20.5) and **2** (173.9 ± 15.6). An incubation concentration of 500 μM has to be used for **1** and **2** in order to reach detectable cellular Ru level, while **3** (103.1 ± 5.8) shows a comparable Ru level after exposure to a much lower concentration (10 μM). The cellular uptake data obtained for complexes **1**−**3** show a clear correlation between

Table 1. IC_{50} Values of Tested Compounds Towards Different Cell Lines[a]

	IC_{50} (μM)			
	HepG2	HeLa	MCF-7	MCF-10
cis-$[Ru(bpy)_2Cl_2]$	> 200	> 200	> 200	> 200
cis-$[Ru(phen)_2Cl_2]$	186.2 ± 6.2	> 200	> 200	> 200
cis-$[Ru(DIP)_2Cl_2]$	106.2 ± 7.6	123 ± 5.4	142.5 ± 6.1	167.8 ± 5.8
1-Py-βC	> 200	> 200	> 200	> 200
1	86.2 ± 12.3	61.2 ± 3.9	102.5 ± 14.5	205.2 ± 12.3
2	50.3 ± 2.2	20.2 ± 1.6	56.7 ± 2.8	133.6 ± 7.2
3	3.5 ± 0.3	1.9 ± 0.2	5.9 ± 0.4	40.6 ± 3.1
4	170.2 ± 12.0	152.1 ± 13.1	260.3 ± 26.3	286.4 ± 9.1
NAMI-A	533.5 ± 34.1	625.8 ± 44.5	619.8 ± 27.8	647.3 ± 41.2
cisplatin	20.2 ± 3.6	16.7 ± 2.5	35.2 ± 4.2	56.2 ± 5.9

[a] IC_{50} values are given in μM, and those of 1-Py-βC, the Ru(II) precursors, **4**, NAMI-A, and cisplatin are included for comparison. Data are presented as mean values ± standard deviations, and cell viability is assessed after 48 h of incubation.

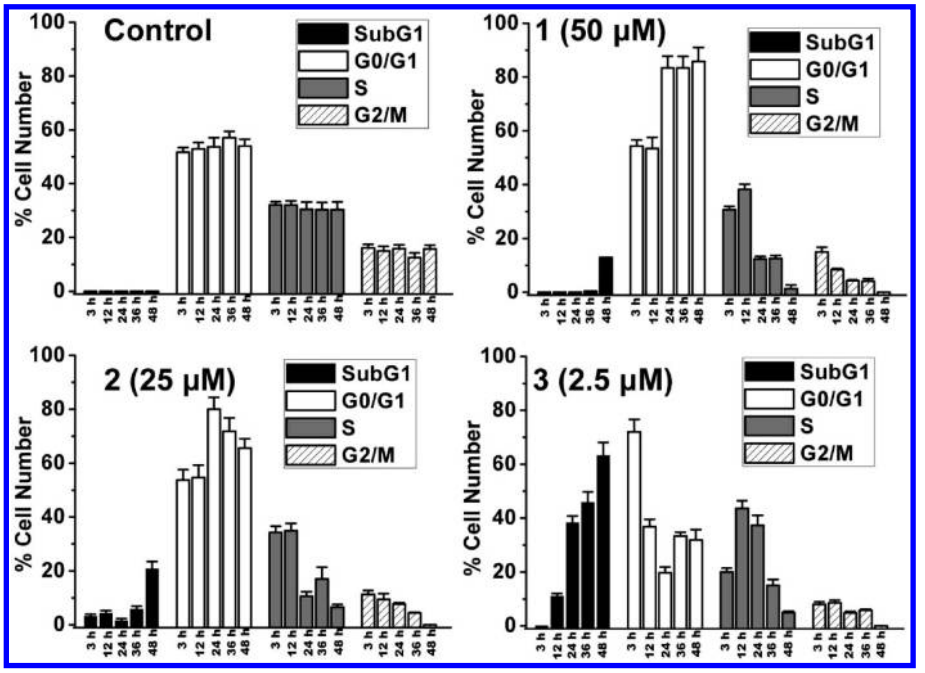

Figure 3. Quantitative cell cycle distribution data for HeLa cells after treatment with **1**−**3**. Data shown are mean values ± standard deviations of three samples for each treatment.

the lipophilicity and the amount of ruthenium associated with the cells.

In Vitro Cytotoxicity. To explore the antitumor potential of the Ru(II) complexes, HepG2 (human hepatocellular liver carcinoma), HeLa, MCF-7 (human breast adenocarcinoma), and MCF-10 (immortalized human breast epithelial) cells were treated with varying concentrations of Ru(II) for 48 h, and cell viability was determined by the MTT (3-(4,5-dimethylthiazol-2-yl)-2,5-diphenyltetrazolium bromide) assay. 1-Py-βC, three Ru(II) synthetic precursors, complex **4**, NAMI-A, and cisplatin were included as controls. The resulting IC_{50} values for the tested compounds are shown in Table 1. The result indicates that, in general, on the basis of calculated IC_{50} values, the following order of in vitro antiproliferative activity of the compounds can be considered: **3** > cisplatin > **2** > **1** > **4** > NAMI-A. The Ru(II) precursors are far more cytotoxic than the corresponding Ru(II) β-carboline complexes against all the cell lines screened. **1**−**3** also show an increased cytotoxic potency if compared with the ligand 1-Py-βC alone, which is inactive against all the cell lines tested (IC_{50} > 200 μM). Notably, complex **3** is more potent than cisplatin against all the cancer cell lines screened (approximately 9-fold more potent than cisplatin in killing HeLa cells), while its cytotoxicity against the normal-like breast epithelial cell line, MCF-10 ($IC_{50} \approx 40.6$ μM), is only slightly higher than that of cisplatin ($IC_{50} \approx 56.2$ μM). NAMI-A shows a very low cytotoxic potency, with IC_{50} values ranging between 533.5 and 647.3 μM, which is consistent with the literature reports.[12]

Cell Cycle Arrest and Induction of Apoptosis. The effect of **1**−**3** on cell cycle was investigated by flow cytometry in PI (propidium iodide) stained cells after Ru(II) treatment for 3, 12, 24, 36, and 48 h (Figure 3 and Supporting Information Figure S13). **1** (50 μM) and **2** (25 μM) cause pronounced G0/G1 arrest after 24 h of incubation (83.4 ± 4.3% and 80.0 ± 3.4% for **1** and **2**, respectively) compared with the vehicle-treated cells (53.7 ± 3.4%). After treatment for 48 h, both **1** and **2** cause an increase of the sub-G1 fraction (0.8 ± 0.1%, 12.9 ± 0.2%, and 20.7 ± 2.8% for control, **1**, and **2**, respectively), an index of apoptotic DNA fragmentation. Notably, **3** (2.5 μM) causes a significant and time-dependent increase in the percentage of cells in sub-G1 phase. After 48 h of incubation, most of the cells treated with **3** (63.2 ± 4.9%) have undergone apoptosis.

To observe the morphologic characteristics of apoptotic nuclei, HeLa cells were stained with Hoechst 33342 after exposure to serial concentrations of **1**−**4** and cisplatin for 24 h and detected by fluorescence microscopy. Representative images of the cells treated with vehicle (1% DMSO) and **3** are shown in Figure 4A. Control cells exhibit homogeneous nuclear staining, and apoptotic cells increase gradually in a dose-dependent manner and display typical apoptotic changes (e.g., staining bright, condensed chromatin, and fragmented nuclei).[34] The percentages of cells showing abnormal nuclei are shown in Figure 4B, and Ru(II) (**1**, 100 μM; **2**, 50 μM; **3**, 3.75 μM; **4**, 50 μM) treatment increases the percentage of abnormal nuclei (**1**, 35.0 ± 2.0%; **2**, 55.3 ± 3.1%; **3**, 86.3 ± 3.5%; **4**, 14.3 ± 1.5%) compared with the vehicle-treated cells (2.3 ± 1.2%).

The activation of cysteine proteases (caspases) is the best recognized biochemical hallmark of both early and late stages of apoptosis.[35] Thus, we determined the effect of Ru(II) treatment on caspase-3/7 activity. HeLa cells were treated with complexes **1**−**4** and cisplatin at serial concentrations for 6 h, after which caspase-3/7 activity was determined using the Caspase-Glo assay. As shown in Figure 4C, treatment of HeLa cells with **1**−**4** and cisplatin results in a concentration-dependent increase in caspase-3/7 activity.

Compared with **4**, more apoptotic nuclei, consistent with higher level of caspase-3/7 activation, are observed when HeLa cells are incubated with **2**, implying that the β-carboline moiety is involved in the cytotoxicity induced by **1**−**3**. It is evident from these studies that **3** displays a significantly higher potency in apoptosis induction than cisplatin does under similar conditions.

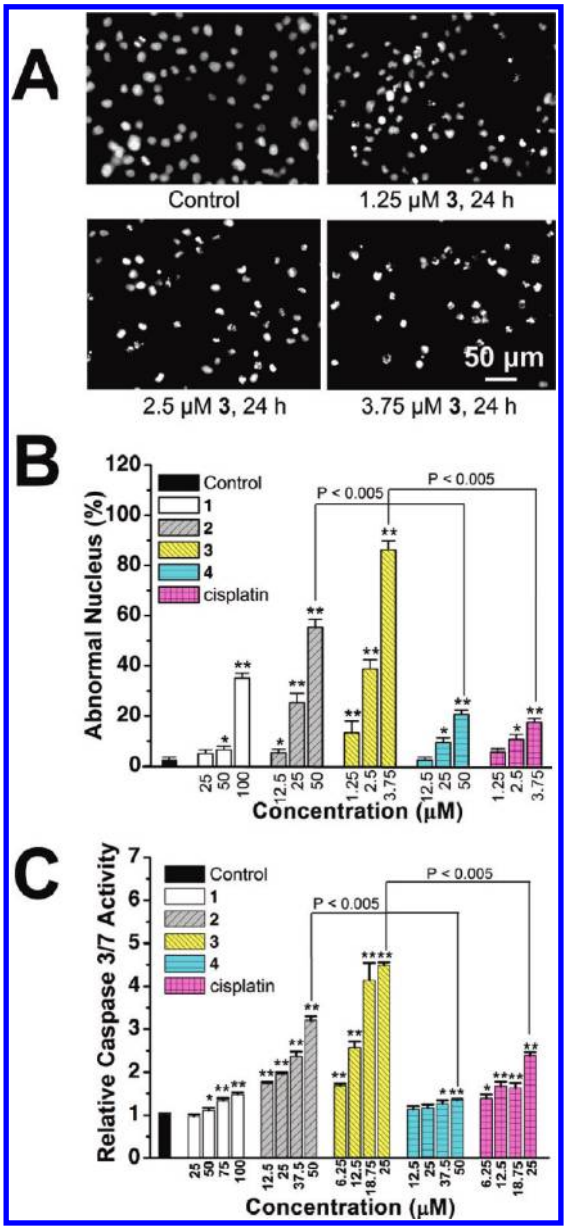

Figure 4. (A) Hochest stained HeLa cells after treatment of **3** at indicated concentrations after 24 h of incubation. (B) Histograms showing the number of cells with abnormal (condensed or fragmented) nuclei. (C) Caspase-3/7 activity after drug treatment for 6 h at indicated concentrations. Data shown are mean values ± standard deviations from three independent experiments: (*) $P < 0.01$, (**) $P < 0.005$, compared with the vehicle-treated cells.

Autophagy Induced by Ruthenium Complexes. TEM is the most convincing method for the analysis of autophagy.[36] Very few autophagical vacuoles are observed, and microvilli are preserved around the cytoplasm in control cells (Figure 5A). Typical autophagic structures, such as autolysosomes and autophagic vacuoles containing cellular material, can be observed in **3**-treated cells (Figure 5B−G). Notably, some of the cells containing autophagic vacuoles simultaneously show morphologies of apoptosis (apoptotic nuclear condensation and fragmentation, Figure 5H).

One of the hallmarks of autophagy is the conversion of the soluble form of LC3 (LC3-I) to the lipidated and autophagosome-associated form (LC3-II);[37] thus, the presence of a punctate pattern of GFP-LC3 expression (GFP-LC3 dots)

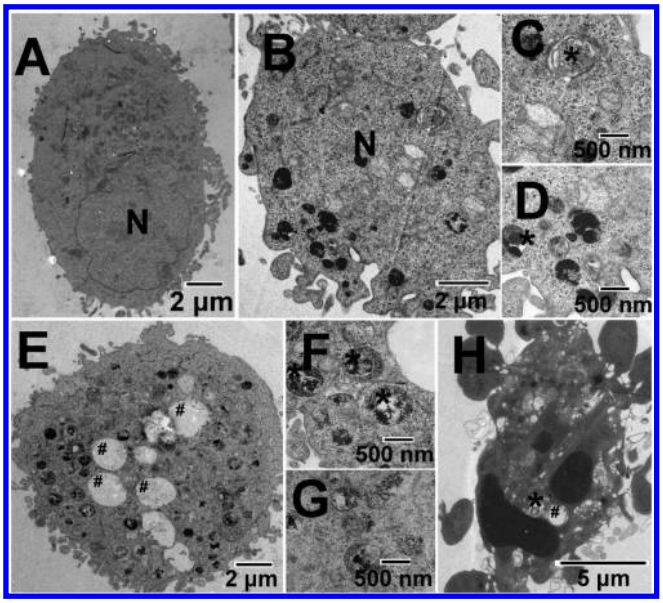

Figure 5. Representative TEM images showing the ultrastructure of HeLa cells treated with vehicle (1% DMSO) (A) or 2.5 μM **3** (B−H) for 12 h. Nuclei are labeled N. Autophagic structures including autolysosomes (*) and autophagic vacuoles (#) are detected in Ru-treated cells. Parts C, D, F, and G are pictures with higher magnification showing detailed autophagic structures.

has been examined to determine whether LC3 is concentrated in HeLa cells after Ru(II) treatment. In cells treated with vehicle (1% DMSO), GFP-LC3 protein is diffusely distributed throughout the cytoplasm, whereas cells treated with **1**−**4** and cisplatin show an increase in number and frequency of GFP-LC3 dots (≥5 dots per cell, Figure 6A). The percentage of autophagy quantified by counting the number of cells showing the punctate pattern of GFP-LC3 in 300 GFP-positive cells is shown in Figure 6B, and 65.4 ± 5.3% of HeLa cells treated with **3** (2.5 μM, 12 h) show GFP-LC3 dots, whereas these autophagic features are detected in only 2.3 ± 1.3% of cells treated with vehicle.

Autophagy is the process of sequestering cytoplasmic proteins into lytic components and is characterized by the formation and promotion of AVOs (acidic vesicular organelles), which can be accessed by AO (acridine orange) staining.[38,39] As shown in Figure 6C, after Ru(II) treatment for 12 h, AO staining reveals an increase in the number of cytoplasmic AVOs, characteristic of autophagy. To quantify the accumulation of the acidic components, flow cytometry was applied to analyze AO-stained cells using the FL3 channel to evaluate the bright red fluorescence and the FL1 channel to evaluate the green fluorescence. As shown in Figure 6D, **1** (100 μM), **2** (50 μM), and **3** (2.5 μM) treatment increases the strength of red fluorescence from 2.2% to 47.2%, 53.3%, and 79.0%, respectively. Both **3** and cisplatin significantly develop AVOs in HeLa cells, and the AVO-inducing ability of **3** is higher than that of cisplatin (62.3%). The formation of red fluorescent AVOs caused by **2** is more pronounced than that caused by **4** (17.7%).

Phosphoinositide 3-kinase (PI3K) is an essential component of core machinery involved in autophagic vesicle formation. 3-MA, the specific class III PI3K inhibitor, can inhibit autophagy at an early stage by preventing the formation of autophagosomes.[40] CQ, a lysosomotropic agent, inhibits autophagy by raising the lysosomal pH, which leads to inhibition of lysosome−autophagosome fusion and lysosomal

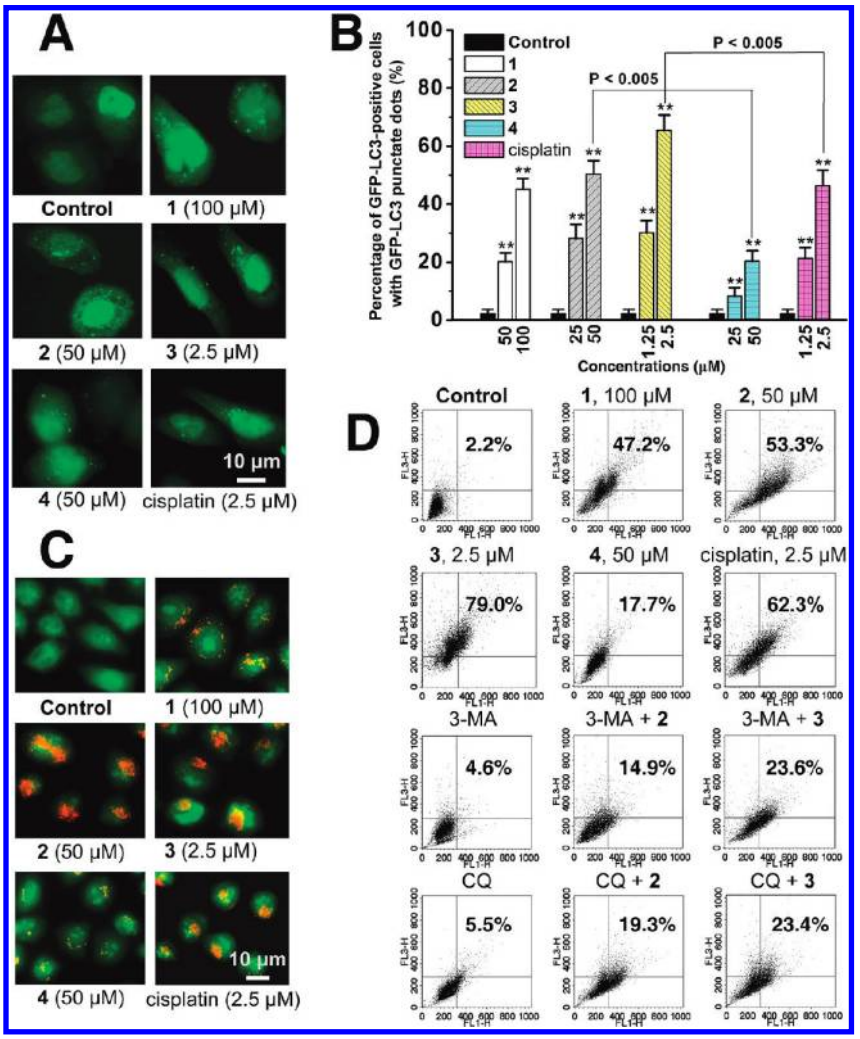

Figure 6. (A) Fluorescence staining of GFP-LC3 in response to drug treatment. (B) Autophagosome formation was quantified after 12 h treatment. Data are presented as percentage of GFP-LC3-transfected cells with punctate fluorescence: (*) $P < 0.01$, (**) $P < 0.005$, compared with vehicle-treated control cells. (C) HeLa cells were stained with AO and examined by fluorescence microscopy after 12 h of treatment. (D) Quantification of AVOs with AO using flow cytometry. HeLa cells were treated with the complexes for 12 h. For inhibitory experiments, cells were treated 3-MA (5 mM) or CQ (2.5 μM) for 1 h and further incubated with or without Ru(II) for 12 h. FL1-H indicates green color intensity, while FL3-H shows red color intensity. Top of the grid is considered as AVOs. Data shown are representative of three independent experiments.

protein degradation.[41] Preincubation of HeLa cells with these inhibitors of autophagy, 3-MA (5 mM) and CQ (2.5 μM), before drug treatment markedly suppresses the induction of AVOs in HeLa cells (Figure 6D).

Induction of Mitochondrial Dysfunction. Mitochondrial dysfunction is involved in both apoptotic and autophagic cell death. Mitochondria play important roles in apoptosis through the release of proapoptotic factors such as cytochrome *c* and apoptosis-inducing factor.[2,42] As a mechanism to maintain genomic integrity in the face of metabolic stress, drug treatment, or radiation, autophagy can selectively remove damaged mitochondria, which are major sites of genotoxic ROS production.[43] Thus, mitochondrial dysfunction was determined by measuring changes in the mitochondrial membrane potential (MMP, $\Delta\Psi_m$) using confocal microscopy and flow cytometry after staining live cells with the cationic dye JC-1 (5,5′,6,6′-tetrachloro-1,1′,3,3′-tetraethylbenzimidazolylcarbocyanine iodide). JC-1 exhibits potential-dependent accumulation in mitochondria, indicated by a fluorescence emission shift from red (~590 nm) to green (~525 nm).[44] Representative images taken by confocal microscope are shown in Figure 7A. **3** (25 μM, 6 h) treatment causes a red to green color shift, indicating loss of MMP, in most of the treated cells. Representative JC-1 red/green ratio signals recorded by flow cytometry in vehicle-treated (1% DMSO) cells and Ru(II)-treated cells are shown in Figure 7B. After 6 h of incubation, **1** (100 μM), **2** (50 μM), and **3** (25 μM) treatment decreases the JC-1 red/green ratio signal from 14.5 ± 1.1 to 1.2 ± 0.2, 1.0 ± 0.1, and 0.6 ± 0.1, respectively.

ROS Accumulation. It is well-known that apoptosis can be triggered by increased intracellular ROS levels,[45] and there is strong evidence that ROS are also involved in the induction of autophagy.[46] Therefore, we investigated whether Ru(II) treatment could increase the ROS level in HeLa cells. ROS accumulation was quantified by the 2′,7′-dichlorofluorescein diacetate (H_2DCF-DA) assay. Confocal microscopic analysis of DCF-stained Ru(II)-treated cells shows significant concentration-dependent increase in intensity of DCF staining compared with the vehicle-treated cells (Figure 8A, left). This result was further confirmed by flow cytometry (Figure 8A, right) and microplate analyzer with DCF staining (Figure 8B). **3** (10 μM) treatment results in a 7.5-fold increase of fluorescence signal compared with the vehicle-treated control, at 6 h post-treatment (Figure 8B).

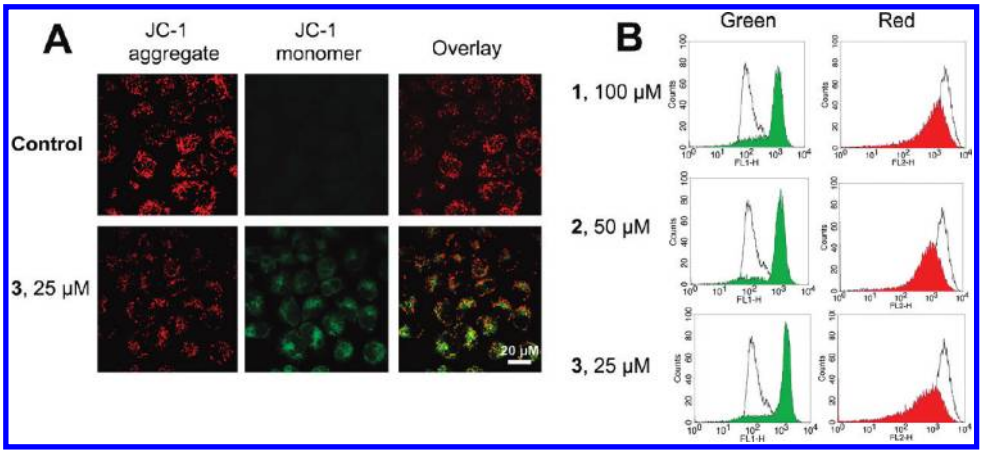

Figure 7. (A) Fluorescence imaging of JC-1 labeled cells taken by confocal microscope. (B) Effects of **1**−**3** on MMP analyzed by flow cytometry. Representative histograms of two independent experiments done in triplicate are shown: (unfilled curve) cultures treated with vehicle (1% DMSO); (filled curve) cultures treated with Ru(II).

Having determined that Ru(II) induced generation of ROS, we proceeded to examine whether ROS played a role in Ru(II)-elicited cell death, autophagy, and apoptosis. We used 4,5-dihydroxy-1,3-benzenedisulfonic acid disodium salt (Tiron, 5 mM) and *N*-acetylcysteine (NAC, 10 mM), two ROS scavengers, and examined their effect on cell viability after Ru(II) treatment. Both Tiron and NAC substantially suppress the ROS accumulation (Figure 8B) and reduce the cytotoxicity of **3** in HeLa cells (Figure 8C). To investigate the involvement of ROS in Ru(II)-induced apoptosis, we monitored drug-induced sub-G1 population in the absence and presence of Tiron and NAC using flow cytometry. There is a decline in the drug-induced sub-G1 population when ROS is inhibited by the antioxidants, suggesting that ROS play a crucial role in induction of apoptosis (Figure 8D). Attenuation of ROS levels by Tiron and NAC significantly decreases the number of AVOs upon Ru(II) treatment (Figure 8E), suggesting ROS also mediate induction of autophagy in HeLa cells. Taking all these results together, we conclude that ROS have an important role in Ru(II)-induced autophagy and apoptosis.

Inhibition of Apoptosis and Autophagy. To gain better insight into the mechanism of Ru(II) cell-killing action, autophagy inhibitors (3-MA and CQ) and caspase inhibitor (z-VAD-FMK) were used to analyze the interconnection between Ru(II)-induced cell death, autophagy, and apoptosis.

First, we determined whether autophagy inhibitors promoted Ru(II)-induced apoptosis using PI staining and flow cytometry. Pretreatment with 3-MA (5 mM) promotes Ru(II)-induced apoptosis, which is demonstrated by the increased percentage of sub-G1 phase cells. Similar results are obtained by pretreatment with CQ (2.5 μM) (Figure 9A and Supporting Information Figure S14). These observations suggest that Ru(II)-mediated autophagy has a cytoprotective role in nature.

Effect of autophagic and caspase inhibitors on Ru(II)-induced cell death is shown in Figure 9B. Cells pretreated with z-VAD-FMK (50 μM) show a marked improvement in cell viability relative to cells treated with Ru(II) complexes alone, suggesting that Ru(II)-induced cell death is caspase-dependent, and autophagy may not be an apoptosis-alternative pathway to induce cell death. In all cases, the CQ/Ru(II) and 3-MA/Ru(II) combinations result in reductions in cell viability when compared with those observed for Ru(II) treatment alone. These data therefore further suggest that Ru(II) complexes stimulate autophagy as a cytoprotective mechanism.

DNA Binding Studies. It has been reported that DNA-damaging agents can activate the intrinsic pathway of apoptosis involving the release of cytochrome *c* and other mitochondrial apoptogenic factors[47] and trigger autophagy simultaneously as a self-defense mechanism.[48,49] Previously, confocal microscopy studies show that **1**−**3** can readily pass the cell membrane and penetrate into the nucleus (Figure 2), so genomic DNA may serve as the target of these complexes. DNA binding studies have been performed to determine whether Ru(II)-induced apoptosis and autophagy are correlated with their abilities to cause DNA damage.

The absorption spectra of **1**, **2**, and **3** in the absence and presence of CT-DNA (calf thymus DNA) are shown in Figure 10A. With increasing concentration of CT-DNA, absorption bands of the complexes display clear hypochromism. The hypochromism (H% = $100 \times (A_{free} - A_{bound})/A_{free}$) of the ^{1}MLCT bands at ~470 nm of **1**, **2**, and **3** are calculated to be about 18.7%, 20.7% and 28.3%, respectively. In order to compare quantitatively the binding affinity of **1**−**3**, the intrinsic binding constants K of **1**−**3** to DNA were determined by monitoring the changes in absorbance at 470 nm (shown in the insets of Figure 10A) using the equation previously described in the literature.[50] The intrinsic binding constants derived for **1**, **2**, and **3** are $(1.08 \pm 0.21) \times 10^6$ M^{-1}, $(1.93 \pm 0.35) \times 10^6$ M^{-1}, and $(3.22 \pm 0.38) \times 10^6$ M^{-1}, respectively, which are in the same range as those reported for Δ-$[Ru(phen)_2(dppz)]^{2+}$ (1.7×10^6 M^{-1}) and Λ-$[Ru(phen)_2(dppz)]^{2+}$ (3.2×10^6 M^{-1}).[51] The changes in emission spectra of **1**−**3** in aqueous solution with increasing DNA concentrations are shown in Figure 10B. As DNA is successively added, an obvious increase in emission intensity can be observed. The emission intensities of **1**, **2**, and **3** increase to about 2.49, 2.97, and 7.48 times of the original intensities, respectively.

Both the electronic absorption titration and fluorescence spectroscopic studies indicate that **1**−**3** have a strong interaction with DNA and the order of DNA binding affinity is **3** > **2** > **1**. The DNA binding affinities of **1**−**3** are consistent with their cytotoxicities and potential to induce apoptosis and autophagy, implying that DNA may be their primary target, and genotoxic stress caused by DNA damage triggers mitochondria-mediated apoptosis and autophagy.

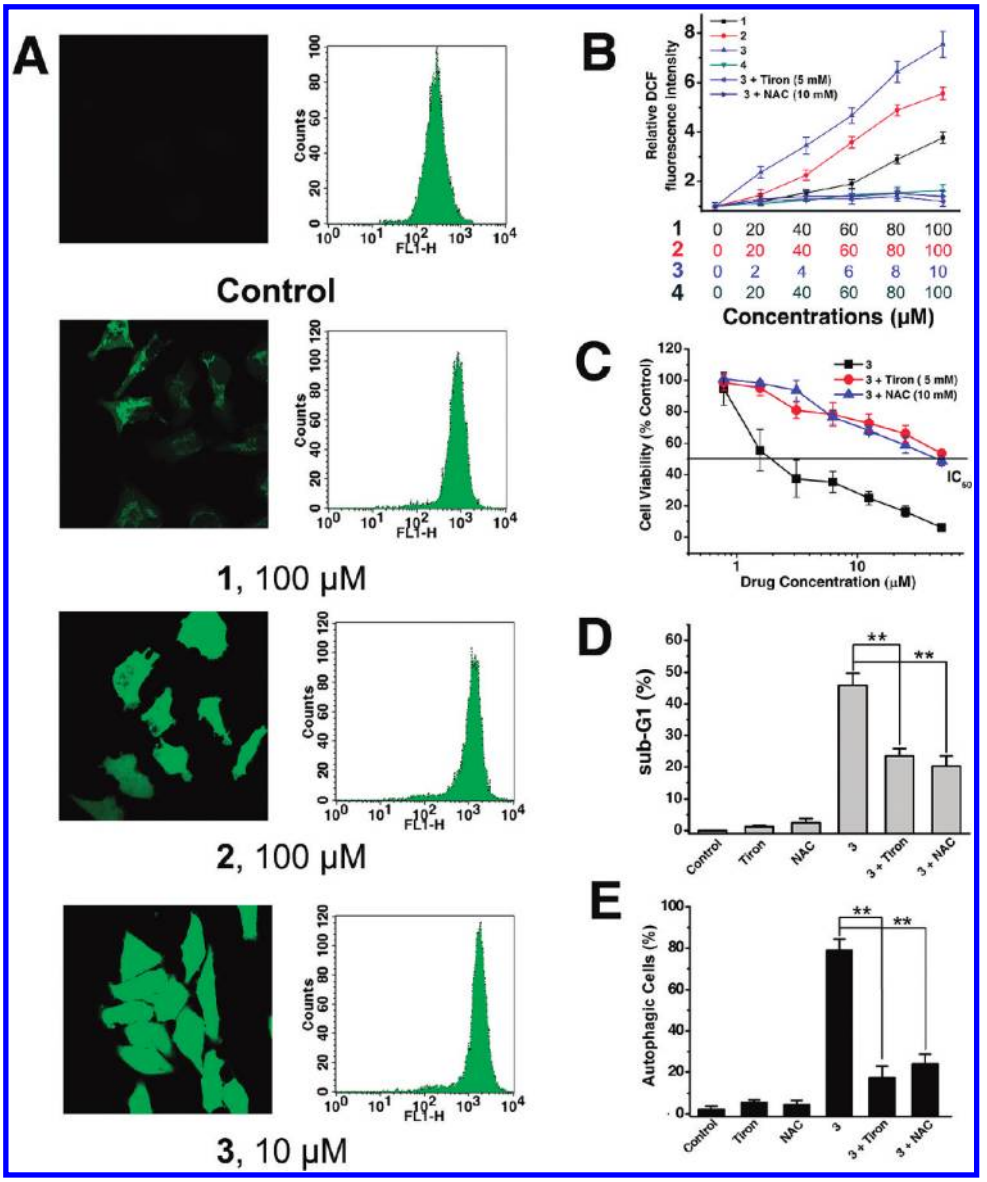

Figure 8. Analysis of ROS production after HeLa cells were treated with Ru(II) for 6 h. (A) The intracellular ROS level was detected by confocal microscope (excitation at 488 nm and emission at 530 nm) and flow cytometry (FL-1 channel; excitation at 488 nm and emission at 525 nm). (B) ROS level is expressed as relative fluorescence intensity measured in a microplate reader after 6 h of Ru(II) treatment with or without antioxidants at the indicated concentrations. Data are presented as mean values ± standard deviations and are obtained in three independent experiments. (C) Effects of Tiron (5 mM) and NAC (10 mM) on **3**-induced cytotoxicity. HeLa cells were exposed to different doses of **3** with or without antioxidants for 48 h. Cell viability was assessed by MTT assay. (D) Attenuating ROS levels by Tiron (5 mM) and NAC (10 mM) reduces the sub-G1 population upon **3** (2.5 μM, 24 h) treatment. (E) Effects of Tiron (5 mM) and NAC (10 mM) on **3**-induced autophagy formation. HeLa cells were exposed to 2.5 μM **3** with or without antioxidants for 12 h. The percentage of autophagic cells was quantified by AO using flow cytometry as described in Figure 7D: (∗) $P < 0.01$, (∗∗) $P < 0.005$, compared with the cells treated with **3** alone.

Discussion and Conclusions

β-Carboline alkaloids are originally isolated from the plant *Peganum harmala*. Powdered seeds of *Peganum harmala* have long been used in herbal formulas of traditional Chinese medicine to cure digestive tract tumors.[52] Because of their affinity with benzodiazepine, imidazoline, serotonin receptors of the central nervous system, β-carbolines display considerable acute neurotoxicity, which hinders their clinical applications as anticancer drugs.[18,52] It has long been recognized that, compared with platinum-based anticancer agents, ruthenium complexes have particularly low general toxicity, allowing administration of larger doses.[8,53] On the other hand, bulky and rigid octahedral ruthenium complexes can serve as structural scaffolds to organize the organic ligands in three-dimensional space.[54] For example, organometallic kinase inhibitors derived from the class of indolocarbazole alkaloids (e.g., staurosporine) can match the size of the active site of targeting kinases and discriminate between otherwise closely related binding sites.[55] In the present study, we use the chemically inert and easily synthesized Ru(II) polypyridyl complexes to complement the molecular diversity of β-carboline derivatives in the quest for the discovery of compounds with superior biological activities (e.g., improved solubility and selectivity, diminished neurotoxicity). We present here the first synthesis of a series of ruthenium-β-carboline complexes that display markedly enhanced cytotoxicities, compared with the original alkaloid.

It has been reported that Ru(II) dipyridophenazine complexes can readily accumulate in the cytoplasm of live cells but

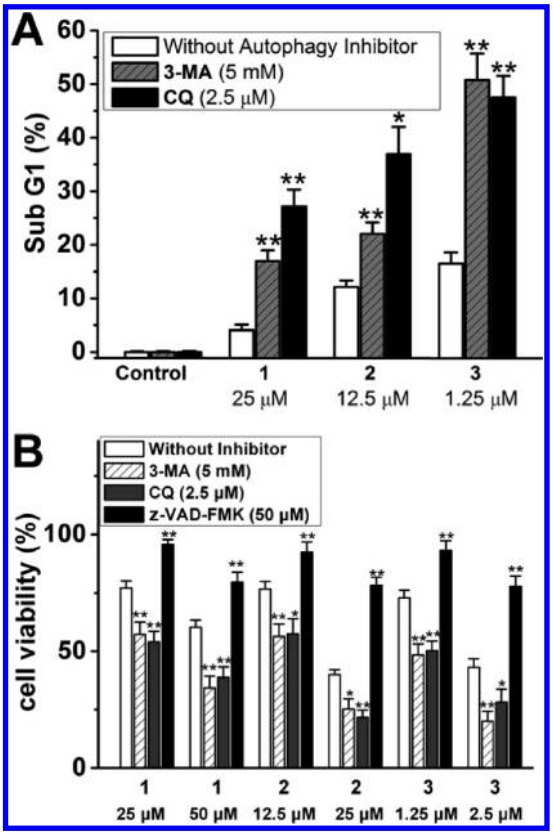

Figure 9. (A) Apoptosis (formation of sub-G1 peak) was determined after cells were treated with Ru(II) for 48 h at the indicated concentrations in the absence or presence of the inhibitors: (*) $P < 0.01$, (**) $P < 0.005$, compared with the percentage of sub-G1 cells for Ru(II) treatment alone. (B) Cell viability was determined by MTT assay after cells were treated with **1**−**3** for 48 h at the indicated concentrations in the absence or presence of 3-MA, CQ, or z-VAD-FMK: (*) $P < 0.01$, (**) $P < 0.005$, compared with the cell viability of Ru(II) treatment alone.

are mostly excluded from the nucleus and mainly localized in the cytoplasm.[26,31] For anticancer agents targeting genomic DNA, nuclear accumulation is highly desirable.[32,33] The subcellular localization of polypyridylruthenium complexes can be greatly influenced by the functional groups (e.g., cell-penetrating peptide,[56,57] fluorescein,[57] phenanthridine,[58] carboxylic groups,[59] and estradiol[30]) attached to the ligand systems. It has been reported that β-carboline analogues can pass through the cell membrane after 1 min of drug exposure and enter the nuclear envelope gradually,[60] and we speculate that may partly explain the nuclear penetrating properties of ruthenium β-carboline complexes. A detailed comparison of complexes **2** and **4** indicates that the coordination of the β-carboline ligand 1-Py-βC to polypyridyl-Ru(II) centers influences their cellular localization and results in more cytotoxic complexes. **2** can readily pass through the nuclear envelope and shows higher ROS, apoptosis, and autophagy-inducing capabilities than **4** does.

Most cancer chemotherapy drugs act through induction of apoptosis.[61] The relationship between autophagy and apoptosis is complex and depends on particular cell type, stimulus, and environment.[62] Evidence has been accumulated to confirm the importance of autophagy in determining the response of tumor cells to chemotherapy.[63] Under certain circumstances, autophagy can manifest a cytoprotective role in drug treatments, such as temozolomide,[39] timosaponin A-III,[64] sulforaphane,[65] tamoxifen,[66] cisplatin,[67] ionizing radiation,[68] and G-quadruplex ligand.[69] Inhibition of autophagy may be therapeutically beneficial in these contexts, as it can sensitize cancer cells to chemotherapies. Autophagy can also play a destructive role in promoting cell death, as in arsenic trioxide-,[70,71] resveratrol-,[72,73] cannabinoid-,[74] and ceramide-induced[75] autophagy. In these cases, the induction of autophagy may be used as a potential therapy for some apoptosis-resistant cancers (i.e., breast and pancreatic cancers). For the first time, we find that ruthenium complexes can induce both autophagy and apoptosis in cancer cells. Such dual properties

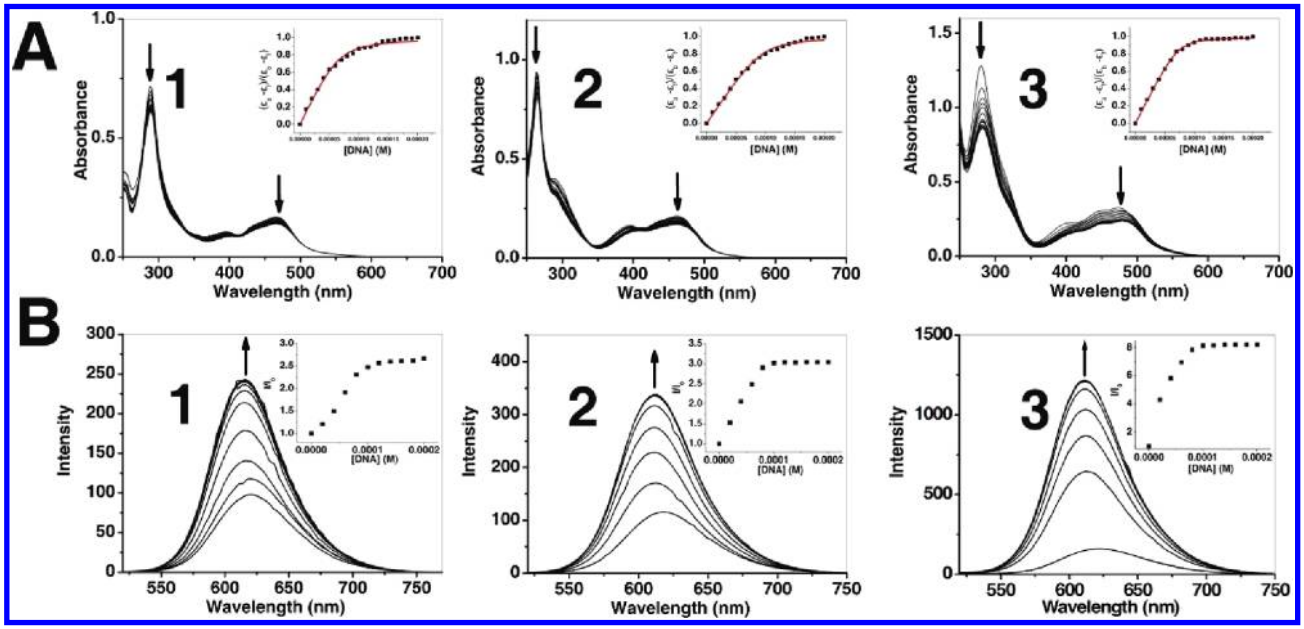

Figure 10. Absorption spectra of **1**−**3** in the absence or presence of increasing amounts of CT-DNA. [Ru] = 10 μM, [DNA] = 0−200 μM from top to bottom. Arrows indicate the change in absorbance upon increasing the DNA concentration. Inset: plots of $(\varepsilon_a - \varepsilon_f)/(\varepsilon_b - \varepsilon_f)$ vs [DNA] and the nonlinear fit for the titration of the complexes with DNA. Also shown are changes in the emission spectra (λ_{em} = 488 nm) of **1**−**3** (10 μM) with increasing concentrations of CT-DNA (0−200 μM).

have never been reported for ruthenium complexes or β-carboline derivatives as far as we know. Inhibition of Ru(II)-induced autophagy by 3-MA or CQ enhances the apoptosis-inducing effect with concomitant increased cell death, suggesting that Ru(II)-induced autophagy is a protective response to the treatment.

In conclusion, our study shows that the combination of ruthenium complexes with β-carboline alkaloids has a great potential for developing new anticancer agents. The most active drug, complex **3**, exhibits higher cytotoxic potency than the widely used clinical chemotherapeutic agent cisplatin. The antiproliferative effects on tumor cells exerted by **1**−**3** are consistent with their intracellular uptake properties, which are significantly enhanced by the increase of lipophilicity with extended π-systems. Further study shows that Ru(II) β-carboline complexes exhibit effective cell growth inhibition by triggering G0/G1 phase arrest and inducing apoptosis through a ROS-mediated mitochondrial dysfunction pathway. In vitro DNA binding studies show that genomic DNA may serve as the primary target of these nuclear permeable complexes. Notably, these newly synthesized Ru(II) β-carboline complexes are dual autophagy- and apoptosis-inducing agents, and they activate autophagy as a cytoprotective response in HeLa cells, and both the apoptosis- and autophagy-inducing activities are at least partially related to ROS accumulation.

Experimental Section

Materials and General Methods. All solvents were of analytical grade. All buffer components were of biological grade and used as received. Ruthenium(III) chloride hydrate (Alfa Aesar), bpy (Alfa Aesar), phen (Alfa Aesar), DIP (Alfa Aesar), cisplatin (Acros), MTT (Sigma), 3-MA (Sigma), CQ (Sigma), PI (Sigma), and NH_4PF_6 (Alfa Aesar) were used without purification. *cis*-$[Ru(N-N)_2Cl_2]\cdot 2H_2O$,[76,77] complex **4**,[78] and NAMI-A[79] were prepared according to reported methods. The purity of synthesized compounds was analyzed via reversed-phase HPLC and was found to be ≥95% pure. Stock solutions of cisplatin (5 mM in PBS) and NAMI-A (10 mM in PBS) were freshly prepared for every experiment. Stock solutions (20 mM) of **1**−**4** were prepared in DMSO, which were proved to be stable for at least 48 h at room temperature as monitored by UV−visible spectroscopy.

Cellular Uptake. Flow Cytometry. HeLa cells in growth medium were seeded in 35 mm tissue culture dishes (Corning) and incubated at 37 °C under a 5% CO_2 atmosphere until 70% confluent. The culture medium was removed and replaced with medium (final DMSO concentration, 1% v/v) containing the Ru(II) complexes at 20 μM. After incubation for 2 h, the cell layer was trypsinized and washed twice with cold PBS (phosphate buffered saline). The samples were raised in 500 μL of cold PBS and analyzed by a FACSCalibur flow cytometer (Becton Dickinson & Co., Franklin Lakes, NJ) immediately. The samples were collected in FL2 channel (excitation at 488 nm and emission at 585 ± 21 nm), and the number of cells analyzed for each sample was 10 000.[30]

Live Cell Confocal Microscopy. HeLa cells were grown on chamber slides to 70% confluence. Complex **3** (5 μM) was added to the culture medium (final DMSO concentration, 0.1% v/v) and incubated for varying amounts of time at 37 °C. The cells were then washed with PBS (2 × 200 μL) and photographed with a Leica TCS SP5 confocal microscope (Leica Microsystems, Wetzlar, Germany) using a planapochromate 63×/NA 1.4 oil immersion objective. The confocal microscope was equipped with an ArKr laser which was used to excite Ru(II) (488 nm excitation, 600−620 nm emission).

GF-AAS (Graphite Furnace Atomic Absorption Spectrometry). HeLa cells were seeded in 60 mm tissue culture dishes (Corning). After overnight incubation, the cells were treated with **1** (500 μM), **2** (500 μM), and **3** (10 μM) for 2 h (final DMSO concentration, 1% v/v). The cells were trypsinized and washed twice with cold PBS, and ruthenium content determined by GF-AAS was presented as ng of ruthenium per mg of cellular protein as described in the literature.[17] All experiments were performed in triplicate.

Autophagy Detection. Transmission Electron Microscopy. HeLa cells (5×10^5) were treated with Ru(II) at 37 °C for 12 h. Cells were washed twice and fixed with 2% glutaraldehyde at 4 °C for 1 h and postfixed with 2% osmium tetroxide. Cells were then dehydrated with sequential washes in ethanol and then embedded in Spurr's resin. The ultrathin sections obtained were mounted in copper grids, counterstained with uranyl acetate and lead citrate, and visualized in an electron microscope (JEM 100 CX, JEOL, Tokyo, Japan). Images were photographed and scanned by using the Eversmart Jazz program (Scitex).

Plasmid and Transfection. Transfection of HeLa cells with GFP-tagged LC3 was performed using jetPEI transfection reagent (Q-Biogen, France) according to the manufacturer's instructions. Cells were transfected with 1 μg of GFP-LC3 expressing plasmid in each well of 24-well plates. After 12 h, cells were treated with **1**−**3** for 12 h. The cells were then fixed with 0.4% paraformalclehyde for 30 min and washed twice with PBS. The fluorescence of GFP-LC3 was viewed, and the rate of GFP-LC3 vacuoles was counted under a fluorescent microscope (Axio Observer Z1, Carl Zeiss, Germany). A minimum of 300 GFP-LC3-transfected cells were counted. Cells treated with vehicle solution (1% DMSO) were included as controls.

Quantification of AVOs with AO. HeLa cells were cultured with medium containing vehicle (1% DMSO) or the complexes for 12 h. For microscopy studies, the cells grown on slides were washed twice with PBS, stained with medium containing 1 μg/mL AO for 15 min, and examined immediately by fluorescence microscopy (Axio Imager Z1, Carl Zeiss, Germany) using 490 nm band-pass blue excitation filters and a 515 nm long-pass barrier filter according to a published protocol.[70] For flow cytometry studies, cells were removed from 60 mm dishes (Corning) with trypsin−EDTA and washed twice with PBS. After being stained with AO for 15 min, the cells were collected in phenol red-free growth medium. Green (510−530 nm) and red (650 nm) fluorescence emission from 10 000 cells illuminated with blue (488 nm) excitation light was analyzed on a flow cytometer (Becton Dickinson, Franklin Lakes, NJ) using CellQuest software.

Intracellular ROS Measurement. After treatment with Ru(II) complexes for 6 h, the cells were incubated with 10 μM H_2DCF-DA (Sigma-Aldrich) for 20 min at 37 °C. The fluorescence intensity of cells was measured by flow cytometry (Becton Dickinson, Franklin Lakes, NJ), confocal microscope (Leica Microsystems, Wetzlar, Germany), and microplate analyzer (Infinite M200, TECAN, Switzerland) with excitation set at 488 nm and emission at 530 nm. When necessary, Tiron (5 mM) and NAC (10 mM) were applied 1 h before Ru(II) treatment and kept in the medium during Ru(II) treatment until the cells were analyzed.

Inhibition of Apoptosis and Autophagy. HeLa cells were preincubated with 25 μM CQ, 5 mM 3-MA, or 50 μM z-VAD-FMK for 1 h before the complexes were added. Percentage of apoptosis was analyzed by flow cytometry, and cell viability was determined by MTT as described in Supporting Information.

Statistical Analysis. All biological experiments were performed at least twice with triplicates in each experiment. Representative results were depicted in this report. Data were presented as mean values ± standard deviations, and comparisons were made using Student's *t* test (two-tailed). A probability of 0.01 or less was considered statistically significant.

Acknowledgment. We thank Prof. Z. P. Chen for providing the GFP-LC3 expression vector. This work is supported by

National Basic Research Program (973 Program, Grant 2007CB815800), International S&T Cooperation Program (Grant 2007DFA30840), State High-Tech Development Program (863 Program, Grants 2006AA090504, 2007AA091401, and 2008AA09Z401), China Postdoctoral Science Foundation (Grant 20080440790), Key Projects of Commission of Science and Technology of Guangdong Province and Guangzhou City, and Project of Sun Yet-sen University Science Foundation. A.X. is a recipient of the "Outstanding Young Scientist Award" from the National Natural Science Foundation of China.

Supporting Information Available: Details of methods; tables of crystallographic data; ORTEP diagram; NMR, ESI-MS, and UV−vis spectra; effects on cell distribution; effects of autophagy inhibitors; and two crystallographic files in CIF format. This material is available free of charge via the Internet at http://pubs.acs.org. X-ray crystallographic data for 1-Py-βC and complex **1** have been deposited in the Cambridge Crystallographic Data Centre under the accession numbers CCDC 771224 and 771225, respectively.

References

(1) Kroemer, G.; Levine, B. Autophagic cell death: the story of a misnomer. *Nat. Rev. Mol. Cell Biol.* **2008**, *9*, 1004–1010.
(2) Hotchkiss, R. S.; Strasser, A.; McDunn, J. E.; Swanson, P. E. Cell death. *N. Engl. J. Med.* **2009**, *361*, 1570–1583.
(3) Mathew, R.; Karantza-Wadsworth, V.; White, E. Role of autophagy in cancer. *Nat. Rev. Cancer* **2007**, *7*, 961–967.
(4) White, E.; DiPaola, R. S. The double-edged sword of autophagy modulation in cancer. *Clin. Cancer Res.* **2009**, *15*, 5308–5316.
(5) Bellodi, C.; Lidonnici, M. R.; Hamilton, A.; Helgason, G. V.; Soliera, A. R.; Ronchetti, M.; Galavotti, S.; Young, K. W.; Selmi, T.; Yacobi, R.; Van Etten, R. A.; Donato, N.; Hunter, A.; Dinsdale, D.; Tirro, E.; Vigneri, P.; Nicotera, P.; Dyer, M. J.; Holyoake, T.; Salomoni, P.; Calabretta, B. Targeting autophagy potentiates tyrosine kinase inhibitor-induced cell death in Philadelphia chromosome-positive cells, including primary CML stem cells. *J. Clin. Invest.* **2009**, *119*, 1109–1123.
(6) Moretti, L.; Yang, E. S.; Kim, K. W.; Lu, B. Autophagy signaling in cancer and its potential as novel target to improve anticancer therapy. *Drug Resist. Updates* **2007**, *10*, 135–143.
(7) Rosenfeldt, M. T.; Ryan, K. M. The role of autophagy in tumour development and cancer therapy. *Expert Rev. Mol. Med.* **2009**, *11*, No. e36.
(8) Bruijnincx, P. C.; Sadler, P. J. New trends for metal complexes with anticancer activity. *Curr. Opin. Chem. Biol.* **2008**, *12*, 197–206.
(9) Vessieres, A.; Top, S.; Pigeon, P.; Hillard, E.; Boubeker, L.; Spera, D.; Jaouen, G. Modification of the estrogenic properties of diphenols by the incorporation of ferrocene. Generation of antiproliferative effects in vitro. *J. Med. Chem.* **2005**, *48*, 3937–3940.
(10) Meggers, E. Targeting proteins with metal complexes. *Chem. Commun.* **2009**, 1001–1010.
(11) Smalley, K. S.; Contractor, R.; Haass, N. K.; Kulp, A. N.; Atilla-Gokcumen, G. E.; Williams, D. S.; Bregman, H.; Flaherty, K. T.; Soengas, M. S.; Meggers, E.; Herlyn, M. An organometallic protein kinase inhibitor pharmacologically activates p53 and induces apoptosis in human melanoma cells. *Cancer Res.* **2007**, *67*, 209–217.
(12) Bergamo, A.; Sava, G. Ruthenium complexes can target determinants of tumour malignancy. *Dalton Trans.* **2007**, 1267–1272.
(13) Hartinger, C. G.; Jakupec, M. A.; Zorbas-Seifried, S.; Groessl, M.; Egger, A.; Berger, W.; Zorbas, H.; Dyson, P. J.; Keppler, B. K. KP1019, a new redox-active anticancer agent-preclinical development and results of a clinical phase I study in tumor patients. *Chem. Biodiversity* **2008**, *5*, 2140–2155.
(14) Peacock, A. F. A.; Sadler, P. J. Medicinal organometallic chemistry: designing metal arene complexes as anticancer agents. *Chem.—Asian J.* **2008**, *3*, 1890–1899.
(15) Suss-Fink, G. Arene ruthenium complexes as anticancer agents. *Dalton Trans.* **2010**, *39*, 1673–1688.
(16) Hotze, A. C. G.; Bacac, M.; Velders, A. H.; Jansen, B. A. J.; Kooijman, H.; Spek, A. L.; Haasnoot, J. G.; Reedijk, J. New cytotoxic and water-soluble bis(2-phenylazopyridine)ruthenium(II) complexes. *J. Med. Chem.* **2003**, *46*, 1743–1750.
(17) Schatzschneider, U.; Niesel, J.; Ott, I.; Gust, R.; Alborzinia, H.; Wolfl, S. Cellular uptake, cytotoxicity, and metabolic profiling of human cancer cells treated with ruthenium(II) polypyridyl complexes $[Ru(bpy)_2(N\text{-}N)]Cl_2$ with N-N = bpy, phen, dpq, dppz, and dppn. *ChemMedChem* **2008**, *3*, 1104–1109.
(18) Cao, R. H.; Peng, W. L.; Wang, Z. H.; Xu, A. L. β-Carboline alkaloids: biochemical and pharmacological functions. *Curr. Med. Chem.* **2007**, *14*, 479–500.
(19) Xiao, S. L.; Lin, W.; Wang, C.; Yang, M. Synthesis and biological evaluation of DNA targeting flexible side-chain substituted beta-carboline derivatives. *Bioorg. Med. Chem. Lett.* **2001**, *11*, 437–441.
(20) Funayama, Y.; Nishio, K.; Wakabayashi, K.; Nagao, M.; Shimoi, K.; Ohira, T.; Hasegawa, S.; Saijo, N. Effects of β- and γ-carboline derivatives on DNA topoisomerase activities. *Mutat. Res., Fundam. Mol. Mech. Mutagen.* **1996**, *349*, 183–191.
(21) Li, Y.; Liang, F. S.; Jiang, W.; Yu, F. S.; Cao, R. H.; Ma, Q. H.; Da, X. Y.; Jiang, J. D.; Wang, Y. C.; So, S. DH334, a β-carboline anti-cancer drug, inhibits the CDK activity of budding yeast. *Cancer Biol. Ther.* **2007**, *6*, 1193–1199.
(22) Castro, A. C.; Dang, L. C.; Soucy, F.; Grenier, L.; Mazdiyasni, H.; Hottelet, M.; Parent, L.; Pien, C.; Palombella, V.; Adams, J. Novel IKK inhibitors: β-carbolines. *Bioorg. Med. Chem. Lett.* **2003**, *13*, 2419–2422.
(23) Al-Allaf, T. A. K.; Ayoub, M. T.; Rashan, L. J. Synthesis and characterization of novel biologically-active platinum(II) and palladium(II) complexes of some β-carboline alkaloids. *J. Inorg. Biochem.* **1990**, *38*, 47–56.
(24) Al-Allaf, T. A. K.; Rashan, L. J. Synthesis and cytotoxic evaluation of the first trans-palladium(II) complex with naturally occurring alkaloid harmine. *Eur. J. Med. Chem.* **1998**, *33*, 817–820.
(25) Alford, P. C.; Cook, M. J.; Lewis, A. P.; Mcauliffe, G. S. G.; Skarda, V.; Thomson, A. J.; Glasper, J. L.; Robbins, D. J. Luminescent metal complexes. Part 5. Luminescence properties of ring-substituted 1,10-phenanthroline tris-complexes of ruthenium(II). *J. Chem. Soc., Perkin Trans. 2* **1985**, 705–709.
(26) Puckett, C. A.; Barton, J. K. Methods to explore cellular uptake of ruthenium complexes. *J. Am. Chem. Soc.* **2007**, *129*, 46–47.
(27) Rillema, D. P.; Jones, D. S.; Woods, C.; Levy, H. A. Comparison of the crystal-structures of tris heterocyclic ligand complexes of ruthenium(II). *Inorg. Chem.* **1992**, *31*, 2935–2938.
(28) Quaranta, A.; Lachaud, F.; Herrero, C.; Guillot, R.; Charlot, M. F.; Leibl, W.; Aukauloo, A. Influence of the protonic state of an imidazole-containing ligand on the electrochemical and photophysical properties of a ruthenium(II)-polypyridine-type complex. *Chem.—Eur. J.* **2007**, *13*, 8201–8211.
(29) Ghezzi, A.; Aceto, M.; Cassino, C.; Gabano, E.; Osella, D. Uptake of antitumor platinum(II)-complexes by cancer cells, assayed by inductively coupled plasma mass spectrometry (ICP-MS). *J. Inorg. Biochem.* **2004**, *98*, 73–78.
(30) Lo, K. K.; Lee, T. K.; Lau, J. S.; Poon, W. L.; Cheng, S. H. Luminescent biological probes derived from ruthenium(II) estradiol polypyridine complexes. *Inorg. Chem.* **2008**, *47*, 200–208.
(31) Puckett, C. A.; Barton, J. K. Mechanism of cellular uptake of a ruthenium polypyridyl complex. *Biochemistry* **2008**, *47*, 11711–11716.
(32) Noor, F.; Wustholz, A.; Kinscherf, R.; Metzler-Nolte, N. A cobaltocenium-peptide bioconjugate shows enhanced cellular uptake and directed nuclear delivery. *Angew. Chem., Int. Ed.* **2005**, *44*, 2429–2432.
(33) Puckett, C. A.; Ernst, R. J.; Barton, J. K. Exploring the cellular accumulation of metal complexes. *Dalton Trans.* **2010**, *39*, 1159–1170.
(34) Yan, Y.; Su, X.; Liang, Y.; Zhang, J.; Shi, C.; Lu, Y.; Gu, L.; Fu, L. Emodin azide methyl anthraquinone derivative triggers mitochondrial-dependent cell apoptosis involving in caspase-8-mediated Bid cleavage. *Mol. Cancer Ther.* **2008**, *7*, 1688–1697.
(35) Li, J.; Yuan, J. Caspases in apoptosis and beyond. *Oncogene* **2008**, *27*, 6194–6206.
(36) Shao, Y.; Gao, Z.; Marks, P. A.; Jiang, X. Apoptotic and autophagic cell death induced by histone deacetylase inhibitors. *Proc. Natl. Acad. Sci. U.S.A.* **2004**, *101*, 18030–18035.
(37) Rubinsztein, D. C.; Gestwicki, J. E.; Murphy, L. O.; Klionsky, D. J. Potential therapeutic applications of autophagy. *Nat. Rev. Drug Discovery* **2007**, *6*, 304–312.
(38) Chen, Y.; McMillan-Ward, E.; Kong, J.; Israels, S. J.; Gibson, S. B. Oxidative stress induces autophagic cell death independent of apoptosis in transformed and cancer cells. *Cell Death Differ.* **2008**, *15*, 171–182.
(39) Kanzawa, T.; Germano, I. M.; Komata, T.; Ito, H.; Kondo, Y.; Kondo, S. Role of autophagy in temozolomide-induced cytotoxicity for malignant glioma cells. *Cell Death Differ.* **2004**, *11*, 448–457.

(40) Seglen, P. O.; Gordon, P. B. 3-Methyladenine: specific inhibitor of autophagic/lysosomal protein degradation in isolated rat hepatocytes. *Proc. Natl. Acad. Sci. U.S.A.* **1982**, *79*, 1889–1892.
(41) Maclean, K. H.; Dorsey, F. C.; Cleveland, J. L.; Kastan, M. B. Targeting lysosomal degradation induces p53-dependent cell death and prevents cancer in mouse models of lymphomagenesis. *J. Clin. Invest*. **2008**, *118*, 79–88.
(42) Wang, C. X.; Youle, R. J. The role of mitochondria in apoptosis. *Annu. Rev. Genet*. **2009**, *43*, 95–118.
(43) Kim, I.; Rodriguez-Enriquez, S.; Lemasters, J. J. Selective degradation of mitochondria by mitophagy. *Arch. Biochem. Biophys*. **2007**, *462*, 245–253.
(44) Nowak, G. Protein kinase C-α and ERK1/2 mediate mitochondrial dysfunction, decreases in active Na^+ transport, and cisplatin-induced apoptosis in renal cells. *J. Biol. Chem*. **2002**, *277*, 43377–43388.
(45) Ozben, T. Oxidative stress and apoptosis: impact on cancer therapy. *J. Pharm. Sci*. **2007**, *96*, 2181–2196.
(46) Scherz-Shouval, R.; Elazar, Z. ROS, mitochondria and the regulation of autophagy. *Trends Cell Biol*. **2007**, *17*, 422–427.
(47) Kaufmann, S. H.; Hengartner, M. O. Programmed cell death: alive and well in the new millennium. *Trends Cell Biol*. **2001**, *11*, 526–534.
(48) Kang, K. B.; Zhu, C.; Yong, S. K.; Gao, Q.; Wong, M. C. Enhanced sensitivity of celecoxib in human glioblastoma cells: induction of DNA damage leading to p53-dependent G1 cell cycle arrest and autophagy. *Mol. Cancer* **2009**, *8*, 66.
(49) Abedin, M. J.; Wang, D.; McDonnell, M. A.; Lehmann, U.; Kelekar, A. Autophagy delays apoptotic death in breast cancer cells following DNA damage. *Cell Death Differ*. **2007**, *14*, 500–510.
(50) Nair, R. B.; Teng, E. S.; Kirkland, S. L.; Murphy, C. J. Synthesis and DNA-binding properties of $[Ru(NH_3)_4dppz]^2$. *Inorg. Chem*. **1998**, *37*, 139–141.
(51) Haq, I.; Lincoln, P.; Suh, D.; Norden, B.; Chowdhry, B. Z.; Chaires, J. B. Interaction of Δ- and Λ-$[Ru(phen)_2DPPZ]^{2+}$ with DNA: a calorimetric and equilibrium binding study. *J. Am. Chem. Soc*. **1995**, *117*, 4788–4796.
(52) Chen, Q.; Chao, R.; Chen, H.; Hou, X.; Yan, H.; Zhou, S.; Peng, W.; Xu, A. Antitumor and neurotoxic effects of novel harmine derivatives and structure-activity relationship analysis. *Int. J. Cancer* **2005**, *114*, 675–682.
(53) Timerbaev, A. R.; Hartinger, C. G.; Aleksenko, S. S.; Keppler, B. K. Interactions of antitumor metallodrugs with serum proteins: advances in characterization using modern analytical methodology. *Chem. Rev*. **2006**, *106*, 2224–2248.
(54) Meggers, E. Exploring biologically relevant chemical space with metal complexes. *Curr. Opin. Chem. Biol*. **2007**, *11*, 287–292.
(55) Maksimoska, J.; Feng, L.; Harms, K.; Yi, C.; Kissil, J.; Marmorstein, R.; Meggers, E. Targeting large kinase active site with rigid, bulky octahedral ruthenium complexes. *J. Am. Chem. Soc*. **2008**, *130*, 15764–15765.
(56) Neugebauer, U.; Pellegrin, Y.; Devocelle, M.; Forster, R. J.; Signac, W.; Moran, N.; Keyes, T. E. Ruthenium polypyridyl peptide conjugates: membrane permeable probes for cellular imaging. *Chem. Commun*. **2008**, 5307–5309.
(57) Puckett, C. A.; Barton, J. K. Fluorescein redirects a ruthenium-octaarginine conjugate to the nucleus. *J. Am. Chem. Soc*. **2009**, *131*, 8738–8739.
(58) O'Connor, N. A.; Stevens, N.; Samaroo, D.; Solomon, M. R.; Marti, A. A.; Dyer, J.; Vishwasrao, H.; Akins, D. L.; Kandel, E. R.; Turro, N. J. A covalently linked phenanthridine-ruthenium(II) complex as a RNA probe. *Chem. Commun*. **2009**, 2640–2642.
(59) Musatkina, E.; Amouri, H.; Lamoureux, M.; Chepurnykh, T.; Cordier, C. Mono- and dicarboxylic polypyridyl-Ru complexes as potential cell DNA dyes and transfection agents. *J. Inorg. Biochem*. **2007**, *101*, 1086–1089.
(60) Tu, L. C.; Chen, C. S.; Hsiao, I. C.; Chern, J. W.; Lin, C. H.; Shen, Y. C.; Yeh, S. F. The β-carboline analog Mana-Hox causes mitotic aberration by interacting with DNA. *Chem. Biol*. **2005**, *12*, 1317–1324.
(61) Pommier, Y.; Sordet, O.; Antony, S.; Hayward, R. L.; Kohn, K. W. Apoptosis defects and chemotherapy resistance: molecular interaction maps and networks. *Oncogene* **2004**, *23*, 2934–2949.
(62) Eisenberg-Lerner, A.; Bialik, S.; Simon, H. U.; Kimchi, A. Life and death partners: apoptosis, autophagy and the cross-talk between them. *Cell Death Differ*. **2009**, *16*, 966–975.
(63) Dalby, K. N.; Tekedereli, I.; Lopez-Berestein, G.; Ozpolat, B. Targeting the prodeath and prosurvival functions of auto phagy as novel therapeutic strategies in cancer. *Autophagy* **2010**, *6*, 322–329.
(64) Sy, L. K.; Yan, S. C.; Lok, C. N.; Man, R. Y.; Che, C. M. Timosaponin A-III induces autophagy preceding mitochondria-mediated apoptosis in HeLa cancer cells. *Cancer Res*. **2008**, *68*, 10229–10237.
(65) Herman-Antosiewicz, A.; Johnson, D. E.; Singh, S. V. Sulforaphane causes autophagy to inhibit release of cytochrome C and apoptosis in human prostate cancer cells. *Cancer Res*. **2006**, *66*, 5828–5835.
(66) Qadir, M. A.; Kwok, B.; Dragowska, W. H.; To, K. H.; Le, D.; Bally, M. B.; Gorski, S. M. Macroautophagy inhibition sensitizes tamoxifen-resistant breast cancer cells and enhances mitochondrial depolarization. *Breast Cancer Res. Treat*. **2008**, *112*, 389–403.
(67) Harhaji-Trajkovic, L.; Vilimanovich, U.; Kravic-Stevovic, T.; Bumbasirevic, V.; Trajkovic, V. AMPK-mediated autophagy inhibits apoptosis in cisplatin-treated tumour cells. *J. Cell. Mol. Med*. **2009**, *13*, 3644–3654.
(68) Paglin, S.; Hollister, T.; Delohery, T.; Hackett, N.; McMahill, M.; Sphicas, E.; Domingo, D.; Yahalom, J. A novel response of cancer cells to radiation involves autophagy and formation of acidic vesicles. *Cancer Res*. **2001**, *61*, 439–444.
(69) Zhou, W. J.; Deng, R.; Zhang, X. Y.; Feng, G. K.; Gu, L. Q.; Zhu, X. F. G-quadruplex ligand SYUIQ-5 induces autophagy by telomere damage and TRF2 delocalization in cancer cells. *Mol. Cancer Ther*. **2009**, *8*, 3203–3213.
(70) Kanzawa, T.; Kondo, Y.; Ito, H.; Kondo, S.; Germano, I. Induction of autophagic cell death in malignant glioma cells by arsenic trioxide. *Cancer Res*. **2003**, *63*, 2103–2108.
(71) Kanzawa, T.; Zhang, L.; Xiao, L. C.; Germano, I. M.; Kondo, Y.; Kondo, S. Arsenic trioxide induces autophagic cell death in malignant glioma cells by upregulation of mitochondrial cell death protein BNIP3. *Oncogene* **2005**, *24*, 980–991.
(72) Opipari, A. W., Jr.; Tan, L.; Boitano, A. E.; Sorenson, D. R.; Aurora, A.; Liu, J. R. Resveratrol-induced autophagocytosis in ovarian cancer cells. *Cancer Res*. **2004**, *64*, 696–703.
(73) Puissant, A.; Robert, G.; Fenouille, N.; Luciano, F.; Cassuto, J. P.; Raynaud, S.; Auberger, P. Resveratrol promotes autophagic cell death in chronic myelogenous leukemia cells via JNK-mediated p62/SQSTM1 expression and AMPK activation. *Cancer Res*. **2010**, *70*, 1042–1052.
(74) Salazar, M.; Carracedo, A.; Salanueva, I. J.; Hernandez-Tiedra, S.; Lorente, M.; Egia, A.; Vazquez, P.; Blazquez, C.; Torres, S.; Garcia, S.; Nowak, J.; Fimia, G. M.; Piacentini, M.; Cecconi, F.; Pandolfi, P. P.; Gonzalez-Feria, L.; Iovanna, J. L.; Guzman, M.; Boya, P.; Velasco, G. Cannabinoid action induces autophagy-mediated cell death through stimulation of ER stress in human glioma cells. *J. Clin. Invest*. **2009**, *119*, 1359–1372.
(75) Guenther, G. G.; Peralta, E. R.; Rosales, K. R.; Wong, S. Y.; Siskind, L. J.; Edinger, A. L. Ceramide starves cells to death by downregulating nutrient transporter proteins. *Proc. Natl. Acad. Sci. U.S.A*. **2008**, *105*, 17402–17407.
(76) Sullivan, B.; Salmon, D.; Meyer, T. Mixed phosphine 2,2′-bipyridine complexes of ruthenium. *Inorg. Chem*. **1978**, *17*, 3334–3341.
(77) Caspar, R.; Cordier, C.; Waern, J. B.; Guyard-Duhayon, C.; Gruselle, M.; Le Floch, P.; Amouri, H. A new family of mono- and dicarboxylic ruthenium complexes $[Ru(DIP)_2)(L_2)]^{2+}$ (DIP = 4,7-diphenyl-1,10-phenanthroline): synthesis, solution behavior, and X-ray molecular structure of trans-$[Ru(DIP)_2(MeOH)_2]$-$[OTf]_2$. *Inorg. Chem*. **2006**, *45*, 4071–4078.
(78) Hartshorn, R. M.; Barton, J. K. Novel dipyridophenazine complexes of ruthenium(II): exploring luminescent reporters of DNA. *J. Am. Chem. Soc*. **1992**, *114*, 5919–5925.
(79) Mestroni, G.; Alessio, E.; Sava, G. New Salts of Anionic Complexes of Ru(III), as Antimetastatic and Antineoplastic Agents. PCT Int. Appl. WO 98/00431, 1998.